JIMMA UNIVERSITY

JIMMA INSTITUTE OF TECHNOLOGY

FACULTY OF MATERIALS SCIENCE AND ENGINEERING

CHAIR OF MATERIALS SCIENCE AND ENGINEERING

MASTER OF SCIENCE PROGRAM IN MATERIALS SCIENCE AND ENGINEERING

Al Doped Graphene as A Promising Anode for Sodium Ion Batteries: A Computational Study

By

Gemechu Abera

A Research Thesis Submitted to School of Graduate Studies of Jimma University in Partial Fulfillment of the Requirements of Master of Science Degree in Materials science and Engineering

September 2022

Jimma, Ethiopia

JIMMA UNIVERSITY

JIMMA INSTITUTE OF TECHNOLOGY

FACULTY OF MATERIALS SCIENCE AND ENGINEERING

CHAIR OF MATERIALS SCIENCE AND ENGINEERING

MASTER OF SCIENCE PROGRAM IN MATERIALS SCIENCE AND ENGINEERING

Al Doped Graphene as A Promising Anode for Sodium Ion Batteries: A Computational Study

By

Gemechu Abera

A Research Thesis Submitted to School of Graduate Studies of Jimma University in Partial Fulfillment of the Requirements of Master of Science Degree in Materials science and Engineering

Advisor: Dr. Mulualem Abebe (Ph.D.)

Co Advisor: Dr. Sathiesh Kumar

September 2022

Jimma, Ethiopia

JIMMA UNIVERSITY

SCHOOL OF GRADUATE STUDIES

JIMMA INSTITUTE OF TECHNOLOGY

FACULTY OF MATERIALS SCIENCE AND ENGINEERING

CHAIR OF MATERIALS SCIENCE AND ENGINEERING

MASTER OF SCIENCE PROGRAM IN MATERIALS SCIENCE AND ENGINEERING

Al Doped Graphene as A Promising Anode for Sodium Ion Batteries: A Computational Study

By: Gemechu Abera Workineh

Approved by Board of Examiners:

Dr. Sintayehu Mekonnen (PhD)

External Examiner   Signature   Date

Dr. Himanshu Panjiar (PhD)

____/____/_____

Internal Examiner   Signature   Date

Dr. Praveen Babu (PhD)

____/____/_____

Chairperson   Signature   Date

Dr. Mulalem Abebe (PhD)

____/____/_____

Main Advisor   Signature   Date
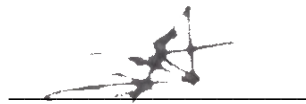
Dr. Sathiesh Kumar (PhD)

____/____/_____

Co- Advisor   Signature   Date

A. Declaration

This thesis, Al doped graphene as a promising anode for Sodium Ion Battery, A computational study, is submitted in candidacy for partial fulfillment of M.Sc. degree in Materials Science and Engineering from Jimma Institute of Technology. Gemechu Abera at the School of Materials Science and Engineering carry out this research work under the supervision of Dr. Mulualem Abebe. The appropriateness of this thesis and its feasibility are believed to right and acknowledged by both the advisors and the advisee.
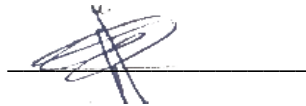
Advisee: Mr. Gemechu Abera _____ ____/____/_____

Signature   Date

Advisor: Dr. Mulualem Abebe _____ ____/____/_____
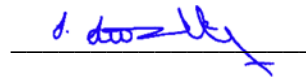
Signature   Date

Co Advisor: Dr. Sathiesh Kumar _____ ___/____/_____

Signature   Date

Faculty approval _____ ____/____/_____

Signature   Date

B. Abstract

Due to abundance, inexpensive, non-toxicity and the similar chemical property as lithium, sodium ion batteries are the best alternative to lithium-ion batteries. Many research were done to improve the energy density and specific capacity of anode for Sodium Ion Batteries (SIBs) by both experimental and computational methods. In this work, Density functional theory (DFT) were used to study the effect of Al dopant on monolayer graphene for application of SIBs anode. Formation energy, adsorption energy, cohesive energy, average voltage as well as open circuit voltage (OCV) of the anode were calculated. The cohesive energy and adsorption energy of the proposed anode were negative, indicates that the proposed 2D Al doped graphene is best candidate as anode for SIBs. Other properties such as electronic structure, Density of State (DOS) and band structure were calculated by using quantum EXPRESSO package. Converged energy cutoff, lattice parameter and K-points grids were optimized. Charge dynamics of the structure were also calculated. Finally, the diffusion barrier of Na on the surface of Al doped graphene is calculated by using NEB method. All the calculation shows that Al doped graphene is a good candidate for SIBs.

Key words: SIBs, Al doped graphene, adsorption, DFT, OCV, band structure, NEB, charge dynamics

C. Acknowledgement

D. Table of Contents

E. List of tables

F. List of Figures

G. List of Acronyms

Lithium-Ion Batteries ………………………………………………………………………... LIBs

Hybrid Electric Vehicles ………………………………….……………………………………. HEV

Sodium-Ion Batteries ………………………………………………………………………... SIBs

Local Density Approximation ……………………………………………………………………. LDA

Generalized Gradient Approximation ……………………………………………………………. GGA

Density Functional Theory ……………………………………………………………………... DFT

Density of States ……………………………………..……………………………………. DOS

Partial Density of States ………………………………………………………………………. PDOS

Born Oppenheimer Approximation ……………………………………………………………. BOA

Projected Augmented Method ………………………………………………………………… PAW

Chloroform or Trichloromethane …………………………………………………………… TCM

Dichloromethane …………………………………………………………………………. DCM

Difluoromethane …………………………………………………………………………. DFM

Self-calculation Field ………………………………………………………………………… SCF

Open Circuit Voltage ………………………………………………………………………... OCV

Diethyl Ether ………………………………………………………………………………… DEE

Ethyl Methyl Ether …………………………………………………………………………. EME

Dimethyl Ether …………………………………………………………………………... DME

Visualization for Electronic Structural Analysis ………………………………………………… VESTA

Crystalline Structure and   Densities …………………………………………………... XCrysDen

Nudge Elastic Path …………………………………………………………………………... NEB

Minimum Energy Path ………………………………………………………………….…… MEP

Potassium Ion Batteries ……………………………………………………………………….. KIBs,

Aluminum Ion Batteries ……………………………………………………………………….. AlIBs

1. INTRODUCTION

At present, environmental contamination is growing at a faster rate with using fossil fuel and coal. It is necessary to develop a new renewable and green energy which can reduce the emission of pollutant. Alternative to fossil fuel energy generation, green and renewable energy generation such as wind energy, solar energy, hydropower has been developed over the last decades. Consequently, there is an increased demand for novel energy storage technology [1-4]. Because of their light weight, great life cycle, superior energy density, incredible electrochemical characteristics, and excellent storage capacity, lithium-ion batteries (LIBs) are one of the most significant energy storage technologies [5-8].

Because of these properties, it is frequently used in portable electronic equipment, hybrid electric vehicles (HEVs), as well as other applications [9-13]. Although LIBs offer several advantages, they are too costly for fixed, large-scale electrical storage, and the restricted supply of Li metal, as well as heating and safety concerns, are important concerns in the use of these batteries [6, 7, 14-16].

Sodium is the most significant substitute to Lithium because of its abundance, cheaper, superior safety features, similar chemical and physical properties as Lithium [4, 11, 15, 17-19]. For instance, trona (Na_2CO_3), the most common sodium mineral is 20-30 times cheaper than zabuyelite (Li_2CO_3), lithium mineral [1, 20]. Due to these reasons, research on sodium ion batteries (SIBs) has accelerated in the recent decades. Because of the abundance of Na element, SIBs are emerged as one of the substitutes of LIBs [18]. However, because the radius of the Na^+ ion is bigger (0.102nm) than that of the Li^+ ion (0.076nm), the potential barrier is higher, resulting in slow Na^+ kinetics. [16]. Also, there are many challenges to the commercialization of SIBs, such as lower cycling stability and low initial Coulomb efficiency, and low energy density [18].
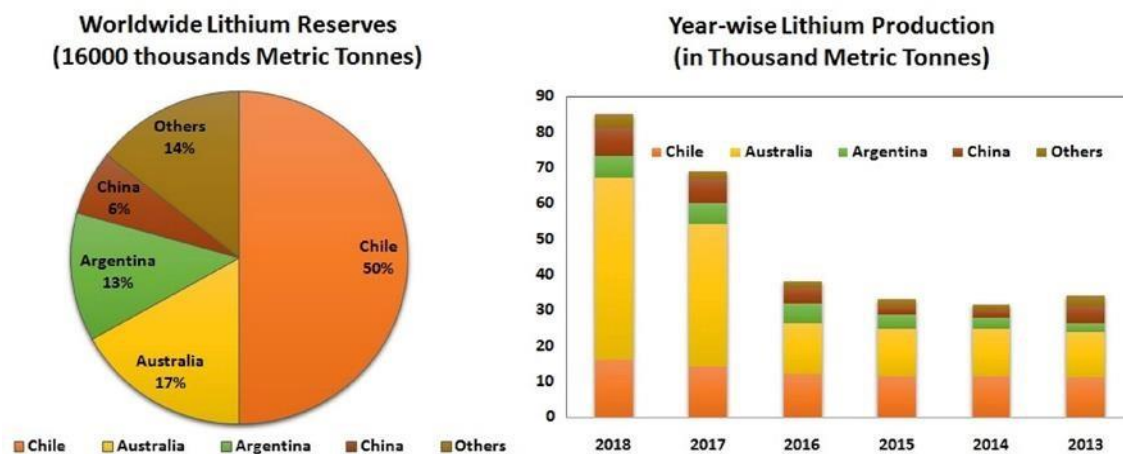
Figure 1. Reserve and production scenario of Li metal

1.1 Sodium ion battery anodes: Overview

SIBs consist of positive and negative electrodes which are connected by immersing into sodium
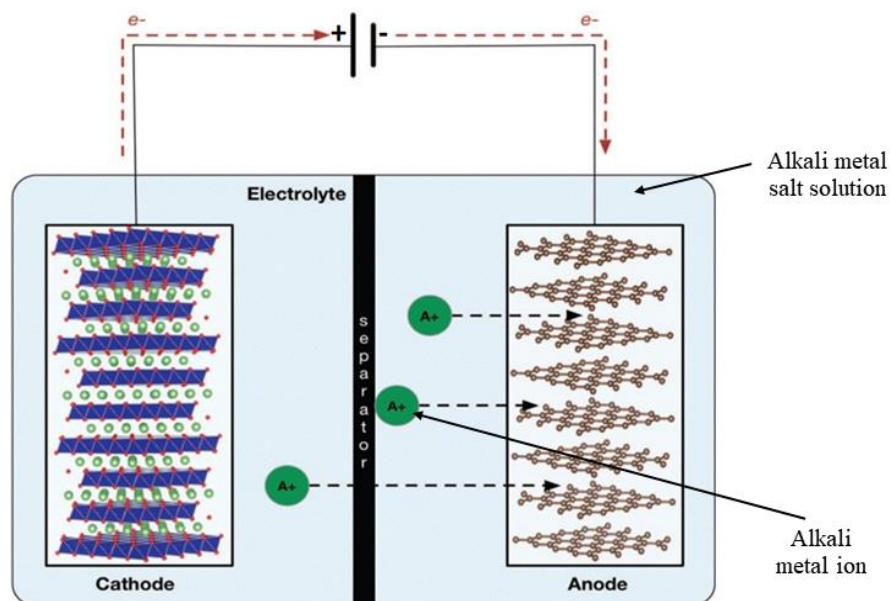
salt electrolytes [21].

Figure 2. Working principle of an alkali ion battery [22]

The SIB faces a significant hurdle due to a scarcity of suitable anode materials. For the last few decades, many scientists try to develop and discover proper electrode materials for SIBs that has a high storage capacity, long lifespan, high-rate capacity, and safety. The development of anode

material is more difficult when compared to cathode materials which can use variety of structure [23, 24].

Today a great number of anode SIBs such as Carbon-based materials, titanates, metal oxide, Conversion Reaction Anode and alloying materials are available [25-27]. However, metallic compounds are limited by their large volume enlargement during sodiation, and titanates cannot meet needed useful use due to their poor capacity. [26]. Conversion reactions anodes, including alloying and metal oxide anodes, exhibit high volume fluctuations during cycling and poor columbic efficiency due to irreversible processes [27].

1.1.1 Structural stability of battery electrode

The structural stability of a battery material is critical to its cycle lifetime. Cohesive energy, formation energy, Gibbs free energy, and the phonon dispersion spectrum can be used to investigate the stability of a battery material.

Cohesive energy: The energy produced when separated free atoms combined to create a chemical compound is known as cohesive energy.

It can be calculated from the following formula

$$E_{coh} = \frac{m \times E(A) + n \times E(B) - E(A_m B_n)}{m + n} \tag{1}$$

Where $A_m B_n$ denotes a compound; m and n denote the number of A and B in the formula; $E(A_m B_n)$, $E(A)$ and $E(B)$ denote the energies of compound $A_m B_n$, isolated atom A, and isolated atom B, respectively; and E_{CO} is the cohesive energy. When the cohesive energy of the structure is higher, it is significantly more stable.

Formation Energy: Formation energy is the energy shift that occurs when a solid or compound is produced by its constituent elements in their normal state. The following equation is used to calculate the formation energy of a compound.

$$E_f = \frac{m \times E'(A) + n \times E'(B) - E'(A_m B_n)}{m + n} \tag{2}$$

While the equation is similar to that of cohesive energy, $E'(A)$ and $E'(B)$ represent the energies of component elements in their normal circumstances rather than separated atoms. The higher the positive formation energy, the more stable the structure is. Because a complex is rarely formed from isolated atoms, the formation energy of a structure predicts its stability better than the cohesive energy.

Gibbs Free Energy: it can be used to compare the stability of isomers or polymorphs at different temperatures or pressures. It may be defined as follows:

$$G = H - TS \qquad (3)$$

$$H = E + PV \qquad (4)$$

Where $G, H, T,$ and S are respectively, Gibbs free energy, enthalpy, temperature, and entropy. E, P and V are internal energy, pressure, and volume.

1.1.2 Theoretical Capacity and Reaction Voltage of Battery

Generally, a battery's power density is proportional to its equilibrium voltage, which is an important commercialization metric for batteries. DFT calculations may be used to estimate the voltage of a new battery structure or to investigate the electrochemical events that occur during the cycling of a battery [28]

A general electrochemical reaction has the form:

$$\alpha A + \beta B \rightarrow \gamma C + \delta D \qquad (5)$$

$\alpha, \beta, \gamma,$ and δ are stoichiometric coefficients. DFT may be used to compute the reaction's energy. Under constant temperature and pressure, the Gibbs free energy of the reaction can be expressed

$$\Delta_r G^\theta = \gamma \Delta_f G_C^\theta + \delta \Delta_f G_D^\theta - \alpha \Delta_f G_A^\theta - \beta \Delta_f G_B^\theta \qquad (6)$$

as

Where $\Delta_r G^\theta$ is Gibbs free energy of the reaction and $\Delta_f G^\theta$ is Gibbs free energy of specific material. At equilibrium voltage, the reaction is reversible. In a battery, $\Delta_r G^\theta$ is equal to the largest nonvolume work that the battery exerts on external systems. If all the Gibbs free energy of the reaction is transformed into electrical energy, the equilibrium voltage can be calculated from the following equation [28]

$$\Delta_r G^\theta = -nFE^\theta \tag{7}$$

where n total number of charge transfer, F faradays constant and E^θ thermodynamic equilibrium voltage under standard state, also called electromotive force. Under isothermal and isobaric condition, $\Delta_r G^\theta$ can be expressed as [29].

$$\Delta_r G^\theta = \Delta_r E^\theta - T\Delta_r S^\theta + P\Delta_r V^\theta \tag{8}$$

Where $\Delta_r E$ is energy of the reaction and $\Delta_r S$ is entropy change. Under constant pressure and room temperate, $P\Delta_r V^\theta$ and $T\Delta_r S^\theta$ terms are negligible [28, 29]. Therefore $\Delta_r G^\theta \approx \Delta_r E^\theta$ is applicable for electrochemical reactions inside the battery.

Additionally, the following equations can be used to compute the theoretical mass energy density (ε_m), volumetric energy density (ε_v), and specific capacity (C) of an electrode [28]:

$$\varepsilon_m = \frac{\nabla_r G^\theta}{\sum M} \tag{9}$$

$$\varepsilon_v = \frac{\Delta_r C^\theta}{\sum V} \tag{10}$$

$$C = \frac{nF}{3.6m} \tag{11}$$

Where M and V are total mole of masses and mole of volumes of the reactants respectively, and m is the mole mass of an electrode material.

1.2 Anode Materials Made from Carbon and Their Performance in Sodium Ion Batteries

Many materials have been developed for SIBs. From those materials, Carbon-based materials, like hard carbon, amorphous carbon, graphite, expanded graphite, and graphene, are by far the most attractive SIB anode materials due to their ease of preparation, relatively inexpensive, stability, and excellent cyclability. [23, 30]. Graphite, which is the best anode for LIBs, cannot be used in SIBs because Na^+ does not intercalate into graphite[27]. Graphite has only recorded an extremely low capacity of 35 mAhg^{-1} for SIBs due to the formation of NaC_{64} because of the larger size of Na^+ and high ionization potential [21, 31].

From these carbon materials, graphene is the best candidate for SIBs anode material because of its good electrical properties, excellent mechanical properties, unique 2D structure and high surface area, high electron conductivity, structural maneuverability, which can enhance the Na^+ storage capacity through surface adsorption and micropore insertion [21, 23, 31].

But pure graphene has poor absorption ability which limits its application as anode materials. So, to enhance electro performance of graphene, point defects, edges, grain boundaries and doping are introduced. Among these, controlled doping of graphene has been achieved in atomic accuracy with good thermodynamics [32].

1.3 Theoretical Simulation

Theoretical methods are used extensively to design and understand material properties in every feature of research. Theoretical methods offer a cost-efficient process to understand the atomic mechanism, complement experimental investigation, screen, and forecast properties.

Since the beginning of quantum theory, the theoretical approaches for studying the properties and the application of materials have been considerably developed. This approach is mainly focused on the Schrödinger equation and studies the electronic properties of solid materials [33].

In investigational fields, the structure-property relationships have been foreseen by vibrational and solid-state NMR spectroscopy by analysis and interpretation of its spectra. Such kinds of progress are focused on the electronic structure of bulk and defect site in semiconductor materials which sever many challenges [34]. For these purposes, Density functional theory (DFT) was being increasingly used as an investigative tool for materials discovery, computational experiments, and crystal structure prediction. The density functional theory (DFT) has proven to be a very powerful tool to theoretically interprets the electronic and chemical properties of materials. The principle is based on the properties of a studied system as a function of the corresponding electron density, which is promising in achieving the goal of maximizing both efficiency and accuracy of a desired electronic properties. After significant development for the past decades, DFT now has become the most widely used theory for electronic structure study [35]. The achievement of DFT is clearly linked to the excellent compatibility of the local density approximation to the simulation of a homogeneous electron gas in the condensed phase. The electron density can be satisfactorily described with the Local Density Approximation (LDA) functional when dispersion or correlation effects are not strong which is common in

solid-state materials. New advanced approximations based on LDA, such as generalized gradient approximation (GGA) or hybrid functionals, were suggested over past years and showed considerable progress at predicting electronic structure of molecules. It is also shown that hybrid functionals also have a better description of the band gap of condensed phase semiconductors. One of the very popular programs of DFT, which implementing many functions is the Quantum ESPRESSO software package. So, this software package is used in this work.

During the last few years, DFT is applied more and more to simulate the structures and explain the behavior of energy storage materials, and the main functionals utilized in battery materials are the GGA functionals, particularly the Perdew–Burke–Ernzerhof (PBE) GGA. Thermodynamic characteristics, electronic structures, reaction kinetics, and ion transport pathways of electrodes and electrolytes for batteries was all computed by using DFT. Compared to experiments DFT simulations demonstrate the benefits of examining reactions at the atomic level and for the efficient assessment of new materials for battery to lower development costs [28].

1.4 Electronic Structure Calculation

The structure of atoms, crystals, molecules, surfaces, and their interactions are computed by Density Functional Theory (DFT) [36]. It relies on Hohenberg and Kohn and Sham approximation that can follow the local density approximation (LDA) or the generalized gradient approximation (GGA) to generate accurate results, for various structural and energetic properties of bulk materials and surfaces, interfaces, and point defects. Molecule physical characteristics are derived from electron assembly mechanisms. To understand these properties, one must investigate electron distributions and interactions which is contained in the electronic wave function governed by Schrödinger's equation:

$$\hat{H}\Psi = E\Psi \tag{12}$$

Which is defining the N-electron Eigenfunction Ψ and eigenvalue E of the Hamiltonian $\hat{H}$. For single electron, Hamiltonian $\hat{H}$ is given by,

$$\hat{H} = \frac{P^2}{2m} + V(r) \tag{13}$$

Where p, m and $V(r)$ represent momentum, mass of electron and potential energy respectively. The permissible values are referred to as eigenvalues since not all energy values are permitted. The functions Ψ which belong to the eigenvalues, and which are a solution of the vibration equation and, in addition, satisfy the boundary conditions, are called eigenfunctions of the differential equation. The non-relativistic Hamiltonian is written as the sum of different kinetic and potential contributing arising from interacting electrons and nuclei:

$$\hat{H} = T_N + T_e + V_{Ne} + V_{ee} + V_{NN} \tag{14}$$

Where T_N, T_e, V_{Ne}, V_{ee} and V_{NN} are kinetic energy of nuclei, the kinetic energy of an electron, interaction potential between nuclei and electrons, interaction potential between electrons and electrons, and interaction potential between nuclei and nuclei.

According to the Born-Oppenheimer approximation (BOA) the nuclei are considered immobile due to their masses are much heavier than the electrons and their kinetic energy is much lower, and the problem is solved by considering only the electronic part of the Hamiltonian. Thus, the electronic Hamiltonian using atomic units given as [37]:

$$\hat{H}_{elec} = -\frac{1}{2}\sum_i \nabla_i^2 - \sum_i \sum_A \frac{Z_A}{r_{iA}} + \sum_A \sum_{j>1} \frac{1}{r_{ij}} \tag{15}$$

Where the first term on the kinetic energy of electron, the second term is the electric potential between the nuclei and the electrons, and the third term is electron-electron repulsion. Although the first two terms are mono-electronic, the third factor, electron-electron repulsion, prevents the many-body issue from being solved analytically. Generally, DFT calculations allow investigating the electronic structure of nanomaterials and thus predicting their fundamental properties, help their characterization, justify the experimental results, and forecast the potential application. The main equation of DFT was explained by Kohn-Sham. In this case there are two theorems which postulate the properties of any system. The first theorem explains as the ground state energy is the unique function of electron density i.e., $E_0 = E (n_o(r))$ while the second theorem describes the electron density that minimize the energy of the system is true ground electron density. Based on these theorems if someone get the electron density of the system it is easily to calculate the ground energy and know all properties of the system at ground states. The overall Kohn-sham equation is given as:

$$\left[-\frac{1}{2}\nabla^2 + V_{ext}(r) + V_H(r) + V_{xc}(r)\right]\varphi_i(r) = \epsilon_i \varphi_i(r) \qquad (16)$$

Where $V_{ext}(r)$, $V_H(r)$ and $V_{xc}(r)$ are external potential, Hartree potential and exchange correlation potential. $\varphi_i(r)$ is Kohn Sham orbital and ϵ_i Kohn Sham eigen energy.

1.4.1 K-points, Space Group and First Brillion Zone

K-point grid is sampling point in Brillouin zone which rises from Bloch theorem. For our calculation the K-points file is used to specify the Bloch vectors (k-points) to sampling the Brillouin zone. There is different mechanism that can specify the k-point grids in the K-POINTS file. These could be through automatically producing regular mesh of points, through the beginning and endpoints of line segments, or as the clear list of points and weights. The actual values of the k-points was optimized by quantum espresso code in SCF calculation, and the optimized values was used for other calculation purposes

Space groups are commonly used to classify the symmetry of crystalline structure which incorporate 32 type of point group symmetry on the arrangement of atoms within the unit cell and 14 types of Bravais lattices of unit cells. There are 230 types of space groups. Within the unit cell, Wyckoff positions are defined to explain site symmetry group that are conjugate subgroups of space group [38-40].

1.4.2 Electronic band structure

In a solid-state physics, the electronic band structure gives the information about a range of energy levels an electron inside the solid can take up, and the band gap is closely associated with electronic conductivity. The band gap of a material is directly related to its conductivity, and the electronic resistance of electrode materials could be analyzed using Density of State (DOS) plots. The DOS is essentially several different states at a certain energy level that electrons are permitted to occupy, that is, the number of electron states per unit volume per unit energy [28]. The physical properties such as optical absorption, electrical resistivity and electrical conductivities are successfully described by Band theory.

1.4.3 Electronic Distribution

Common way of explaining electronic structure is the electronic/charge distribution derived from DFT calculations. The electronic structures of the electrode materials and the chemical environment of the atoms are easily visible in charge distribution, which are difficult to measure using tests [28].

1.5 Charge Distribution Analysis

Materials' properties are governed through their electronic structure, and charge distribution which is a crucial element of that structure. The most straightforward approach to define that distribution is to use partial atomic charges. They give information about charge transfer, charge delocalization, and the type of interaction between atoms [41]. This type of information may be employed to better understand the way molecules and materials interact in terms of their physical, electrical, and magnetic characteristics [42-44]. A wave function can be used in a variety of ways to calculate net atomic charges. Three general classes may be identified:

(i) population analysis, consisting of Mulliken charges, Löwdin charges, [45], and natural charges [46]

(ii) partitioning the electron density, consisting of Bader charges [47, 48], Hirshfeld charges [49], DDEC charges, [50], and CM5 charges [51]. and

(iii) electrostatic fitting, which includes the MerzKollman method [52].

According to Bader charge analysis, which is also called atoms-in-molecules theory, molecules are divided into atoms by zero flux surfaces [47, 48, 53]. A zero-flux surface is a two-dimensional surface on which the charge density crosses the surface at a minimum. The total charge existing within each atom's atomic volume (Bader volume) is known as the Bader charge [47]. Although the approach is mathematically efficient, it has been criticized for not reliably generating electrostatic potentials and dipole moments when atomic charges are retained without incorporating higher multipole moments on each atom [54].

1.6 Minimum Energy Path (MEP)

One of the goals of this research is to better understand the Na diffusion and energy barrier on the surface of Al doped graphene. Finding the lowest energy route for a group of atoms to change from one stable configuration to another is a common and significant issue in theoretical

chemistry and condensed matter physics. [55, 56]. This is often referred to as the minimum energy path (MEP). It is frequently used to define a 'reaction coordinate' for transitions like chemical reactions, molecule conformation changes, or solid diffusion processes. The saddle point, which designates the energy barrier for the migration, is the potential energy maximum along the MEP. It is critical to determine the minimum energy path (MEP) for the corresponding migration process in order to achieve the desired barrier for possible diffusion paths. There are several methods for determining MEP for a specific reaction such as Drag Method [57], Nudge Elastic Method (NEB) [55, 57, 58], Climbing Image NEB (CI-NEB) Method [57, 59], Conjugate Peak Refinement (CPR) Method [57], The Ridge Method [57, 60], The Dewar, Healy and Stewart (DHS) Method [57, 60], and The Dimer Method [57, 60] .

1.6.1 Nudge Elastic Band Method (NEB)

Nudge Elastic Band Method (NEB) is one of the effective way to find MEP for various reaction such diffusion of atomic hydrogen on metal surfaces [61], twin nucleation in Ti [62], diffusion of Li and Na ion 2D materials [63], sodium diffusion on 2D transition metal tellurides [64] and etc.

The technique has been used both in conjunction with electronic structure calculations, particularly plane wave-based DFT calculations, and in conjunction with empirical potentials [59]. The MEP is found by constructing a set of images (duplicates or replicas) of the system, typically on the order

of 4–20, between the initial and final state [57, 59, 62]. In other words, NEB describes the movement of atoms from an initial stable state to a final stable state using as little energy as possible. There may be several reaction pathways connecting the reactants and products, and NEB selects the one that requires the least amount of energy. The NEB method is distinguished from other elastic band methods by a force projection that ensures that the spring forces do not interfere with the convergence of the elastic band to the MEP and that the true force does not affect the distribution of images along the MEP [59]. The NEB method is distinct from others in that it
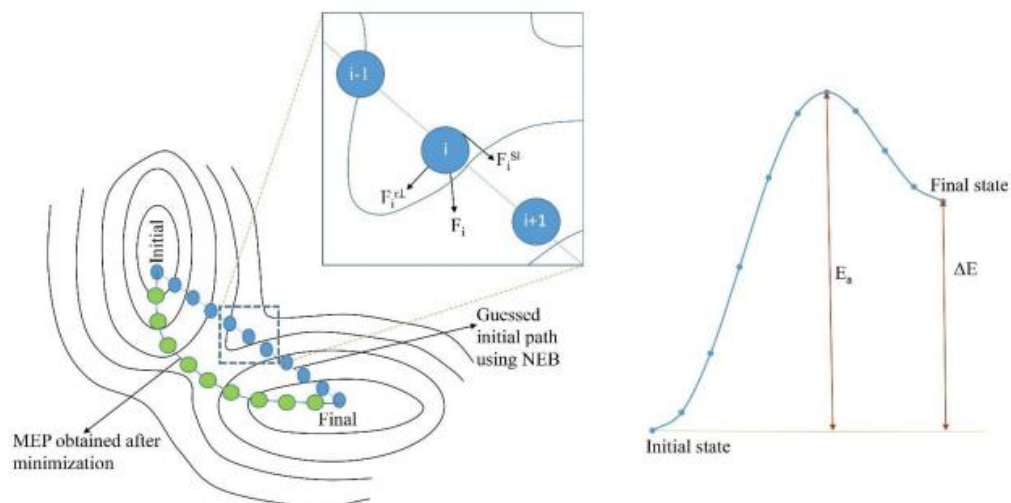
provides not only an estimate of the saddle point, but also a more global view of the energy landscape, such as whether more than one saddle point is found along the MEP [57].

Figure 3. A schematic representation of nudged elastic band (NEB) method [62]

In this study NEB was used to study the diffusion of Na on the Al doped graphene surface. Previously, this method is used to study many types of anode materials for batteries like bismuthene as anode material for alkali-metal ion battery [65], diffusion of alkali atoms on BeN dual doped graphene [66], diffusion of Na on heteroatom doped graphene [67] etc.

1.7 Statements of Problem

Even though there are many anodes developed for SIBs, they suffer from many problems such as over expansion, low cycling, low specific capacity, and low energy density. To overcome these challenges, the developments of anodes based of graphene is highly investigated in the recent year. But due to large energy barrier of sodium on pristine graphene, their application is still facing a problem. By doping graphene sheet, the adsorption of sodium on its surface increases.

1.8 Scopes

The focus of these thesis is the investigation of the effects of Al dopant on graphene as anode materials for SIBs. Formation energy, cohesive energy, and adsorption energy of the structure were calculated. OCV of the electrode were calculated by using first principle calculation based on density functional theory (DFT). This work is limited to theoretical study and enhancement of doped graphene with Al by simulating at atomic level and electronic scale. It does not involve any experimental work.

1.9 Objectives

1.9.1 General Objective

The main objective of this research is to study the effect of doping of Al on graphene as anode for sodium-ion battery.

1.9.2 Specific Objective

- To optimize parameters such as energy cutoff, k-points, and charge density

- To calculate formation energy for doped graphene

- To calculate band structure, DOS, and charge distribution of doped graphene

- To calculate adsorption energy, OCV, average voltage and specific capacity of the adsorbed Na ions

- To calculate charge dynamics of doped graphene and absorbed sodium ion on the doped graphene

- To calculate MEP and diffusion barrier of Na ion on doped graphene

2. LITERATURE REVIEW

2.1 Introduction

Since its discovery in 2004, Graphene has become a topic of strong theoretical and experimental interest in research area [68]. One area of graphene study area is its potential application as energy storage material. It may be used as an anode for a variety of rechargeable batteries such as LIBs [69, 70], potassium ion batteries (KIBs) [32, 69, 71], aluminum ion batteries (AlIBs) [71] and SIBs [69, 71, 72].

When we charge and discharge secondary battery, based on the current direction, ions concentration rises or falls. These processes cause the composition and structural alteration of the anode material [73].

Electronic transport in electrodes, ion transport in bulk electrolyte and electrolyte-filled pores, solid-state diffusion of ions in active materials, and electrochemical reactions at the electrode/electrolyte interface are all factors that affect high-rate capacity in rechargeable batteries [3, 20].

The ability of alkali ions to move in the host crystal of the cathode and anode, the electrolyte, and the electrode electrolyte interface determines the performance of a rechargeable alkali-ion battery. Any part of the battery with poor alkali transfer has a reduced rate capability and practical capacity. [22]. Electrode materials should have good ionic conductivity to exhibit highly efficient battery operation. Conductivity plays a key role in intercalation/deintercalation-based energy storage devices where charge transport of Na^+ ions take place within the electrode materials. Often it discovered that a significant drop in battery performance at high charge/discharge rate is caused by slow movement of Na^+ ions through the material [74]. Fundamental problem in SIBs is the lack of good anode materials. Graphite anodes commercially used in LIBs cannot be used in SIBs, as Na does not intercalate into graphite [24, 27]. Much effort has been made during last decade to find appropriate materials for SIBs to increase the performance of its anodes. Since graphite is not appropriate, researchers have proposed metallic

oxides as TiO_2, MnO_2 and NiO as anode materials with higher theoretical capacities. Then unfortunately, these materials have inadequate electrical conductivity and an unstable chemical structure during the charging and discharging process, which leads to unnecessary cycling performance [24]. The large gravimetric and volumetric specific capacities of alloy-type anodes make them ideal for high-energy SIBs. But they are suffering from huge irreversible capacity, enormous capacity fading, severe volume expansion and inadequate cycling stability[18]. Many studies are focusing on 2D materials to solve the above issues. Among these 2D materials, graphene is the most attractive anode for SIBs because of its large surface area [3, 75], low cost [76], chemical stability and high electronic conductivity [75, 77], nontoxic and good thermal stability.

2.2 Conceptual Framework

In a recent year, theoretical capacity of SIBs anodes based on graphene are improved by many mechanisms such as doping with heteroatom elements like nitrogen, boron, and fluorine. Because of its unusual two-dimensional honeycomb structure and exceptional electrical capabilities, graphene has attracted the attention of a large scientific community, i.e., very long pathway for charge carriers and phonons, and therefore extremely high charge carrier mobility and thermal conductivity[78, 79].

An efficient manner to change the property of graphene is chemical doping [72]. Since group III elements are electron deficient, doping with these elements decreases adsorption energy makes adsorption more energetically favorable.

2.3 DFT Study of Sodium Ion Battery Anodes

The GGA functionals, particularly the Perdew–Burke–Ernzerhof(PBE)GGA, have been widely employed in battery materials research in recent years to model the structures and explain the activities of energy storage materials [28]. DFT is used to figure out how to determine the thermodynamic characteristics, electronic structures, reaction kinetics, and ion transport pathways of electrodes/electrolytes in batteries. DFT simulations outperform experiments in terms of investigating reaction processes at the atomic level and virtual screening novel battery materials to save development costs [28, 80].

DFT may be used to either confirm the results gained from the experimental analysis or to determine among those options which were left open. DFT offers a strong relationship between theory and experiment by calculating a wide variety of molecular characteristics, which frequently leads to valuable insights regarding the geometric, electronic, and spectroscopic aspects of the systems under study [81].

2.4. Anode Materials for SIB Anode

The lack of excellent anode materials is a major challenge in SIBs. Graphite cannot be used as anode for SIBs because Na does not intercalate into graphite. This challenge inspires the examination of a wider range of anode materials for SIBs, such as carbonaceous anodes, alloying anodes, Conversion reaction anodes and sodium titanium oxide anodes [27].

One of the most studied anode materials for SIB is graphene. Many elements, such as boron [67, 72], nitrogen, sulfur and phosphorous [67], can be doped into graphene for use in SIBs.

2.5 Some Application of Al doped Graphene from DFT Perspective

In the past years, many research have been done on the application of doped graphene with Al by using DFT. DFT have successfully predicted the application of Al doped graphene on sensors, removal of toxic substance from environment, hydrogen storage and etc.

Ali Shokuhi Rad studied Al doped graphene as a sensor for some ether molecules such as DEE, EME, and DME, which are very toxic and adsorbent for some halomethane compounds such as Chloroform or trichloromethane (TCM), dichloromethane (DCM), and difluoromethane (DFM). He proves these molecules are absorbed on the surface of Al doped graphene and it can be used as sensor for detection of these molecules [82, 83].

Y.L. Tian, J.F. Ren, W.W. Yue, M.N. Chen, G.C. Hu and X.B. Yuan from Shandong Normal University, China also studied adsorption of chloroform on the surface of Al-doped graphene. They prove that interaction between graphene and chloroform is enhanced by Al doping [84].

In general, Al doped graphene is widely studied for the application of removal of toxic gases such as SO_3 [85], CO and CO_2 [86-89], NH_3 and CH_2 [87], H_2CO [90] , SO_2 [91], and HCN [92]. They proved Al doped graphene can absorb those harmful gases.

16

Another application of Al-doped graphene is to remove F^- and HF molecules from waste water. According to Tao Chen, Libao An, and Xiaotong Jia Al-doped graphene is suitable material for F^- adsorbent [93]. By using DFT Diega Cortés-Arriagada, and Alejandro Toro-Labbé investigated the potential application of Al and Fe doped graphene as very useful adsorbent material for the elimination of harmful methylated arsenicals compounds (such as MMA and DMA) in their trivalent and pentavalent forms, as well as thiolated arsenicals [94]

Al doped graphene is also useful for energy storage devices. Jian Gu et al investigated the hydrogen storage mechanism on Ni and Al doped graphene composites [95].

3. COMPUTATIONAL METHODS

In this work, the overall calculations were performed under different category. First the lattice parameter, energy cutoff and k points (Brillion zone sampling) are optimized. Then the cell was relaxed to get the minimum energy of the system before doing the other calculation. Graphene is a single layer of graphite which has hexagonal crystal structure (where $a = b = 2.46$Å and $\alpha = \beta = 90^o$, $\gamma = 120^o$) and space group of $194, P63/mmc$ [96]. It has two atom per unit cell.

We used 4×4 supercell for both doped and pristine graphene. For doped graphene, one carbon atom is substituted by one Al atom which corresponds to 3.125% of substitution.

During lattice constant optimization, k points were kept constant at $4 \times 4 \times 1$ and cutoff energy were kept at 400eV. After minimum energy were reached, the optimum value of lattice parameter was taken. Then, to optimize k points, we use the optimum value of lattice constant while keeping cutoff energy at 400eV. Finally, by using the optimum value of k points and lattice dimension, the cutoff energy was optimized.

All calculations in this work were done by DFT with projected augmented wave (PAW) method. The approach is based on an iterative solution of the Kohn-Sham equation of the density functional theory in a plane-wave set with the projector-augmented wave (PAW) pseudopotentials [97]. The projector-augmented wave method (PAW) was used to describe the ion–electron interaction [69] by using QUANTUM EXPRESSO code. The periodic boundary condition was applied in three directions (x, y and z) [98]. Cell optimizations were made to completely relax the pristine graphene sheets in terms of lattice parameters and ion sites [67]. In order to avoid periodic image interaction between the two nearest neighbor unit cells, the vacuum was set to 20 Å in the z direction [69, 99]. The generalized gradient approximation (GGA) with Perdew–Burke–Ernzerhof (PBE) functional method was applied to describe the electron-electron exchange correlations [67, 69]. The interactions between valence electrons and ions was described with the projector augmented wave (PAW) pseudo-potentials [100]. The k-points was generated by using the general Monkhorst-Pack scheme for the Brillouin zone sampling and k-points was used for structural configuration optimization and Density of State

(DOS) [67]. After optimization of k-points, lattice and converged kinetic energy cutoff electronic properties of pristine and Al doped graphene was calculated. The band structure of pristine and Al doped graphene was calculated by using $8 \times 8 \times 1$. For DOS, a dense k point of $18 \times 18 \times 1$ was used.
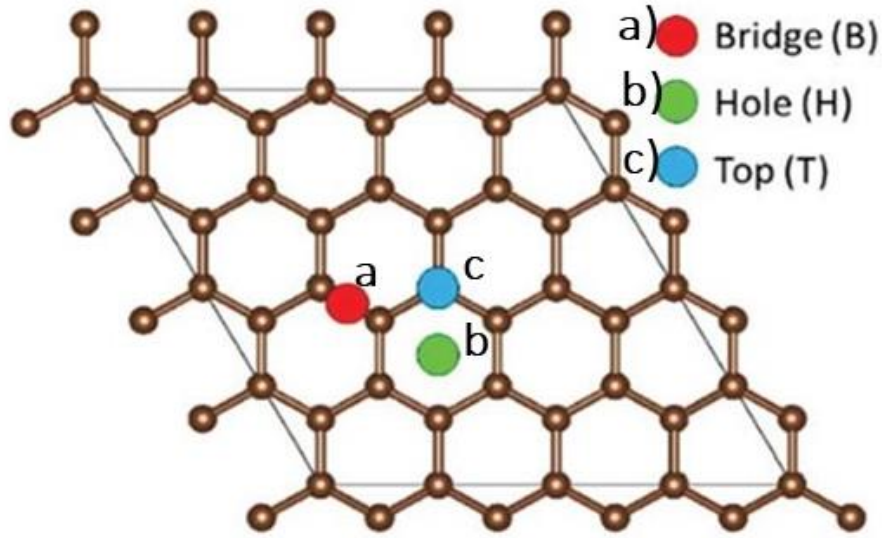
Figure 4. Metal adsorption site on the graphene surface. a) metal adsorption over carbon–carbon bond on the bridge position (Bridge), b) metal adsorption over the carbon atom (Top), and c) metal adsorption over the center of the hexagonal C_6 ring [69].

A 4×4 supercell will be used for the pristine graphene surface calculations, after metal adsorption, and carbon vacancy defect formation energy convergence. To model the adsorption of Na on the graphene, three inequivalent metal adsorption locations was considered, bridge site(B) above a C–C bond, above of a carbon site (T) or center of C_6 unit [69]. The formation energy of doped graphene was calculated as follows.

$$E_F = E_T + n\mu_C - E_g - m\mu_{Al} \tag{17}$$

where E_T is total energy of graphene sheet after doping, n is number of C atoms and m is the number of Al atoms, E_g is total energy of pure graphene, μ_c and μ_i are the energy of carbon atoms and Al atoms respectively [101]. Adsorption energy of Na atom was calculated by using the following equation

$$E_{ad} = \frac{[E_{tot} - (E_{AlC31} + nE_{Na})]}{n} \qquad (18)$$

where E_{ad}, E_{AlC}, E_{Na}, E_{tot} and n represent the adsorption energy, the energy of the Al doped graphene, the energy of the Na atoms, energy of the Na absorbed on Al doped graphene and number of adsorbed Na atoms respectively.

The stability of Na-adsorbed structures in different sodium concentrations is investigated by the cohesive energy, calculated as

$$E_{coh} = \frac{[E_{tot} - (mE_C + nE_{Al} + lE_{Na})]}{m + n + l} \qquad (19)$$

where E_{coh}, E_{tot}, E_C, E_{Al}, E_{Na}, are, respectively, cohesive energy, energy of adsorbed structure, carbon atom, aluminum atom, and sodium atom. m, n and l refer to the number of carbon atoms, aluminum atoms, and number of sodium atoms, respectively. VESTA and XCrysDen used for visualization of the structure.

Finally, Nudge Elastic Band (NEB) was used to study diffusion of Na on the surface of Al doped graphene.

4. RESULT AND DISCUSSION

The system was modeled as 4×4×1 graphene supercell which have 32 carbon atoms. One carbon atom is replaced by aluminum (AlC_{31}) which correspond to 3.125% (atom percent). In order to prevent the interaction between graphene sheets, a vacuum space of 15 Å was created in vertical direction.

4.1 Optimization of Crystal Structure

First principle calculation, which is based on the quantum mechanics concept, is a method for instantly determining physical attributes from fundamental physical quantities like mass, charge, and Coulomb force of an electron. It is based on the information of the crystals such as crystal structure, plane-wave energy cutoff, k-point grids, and lattice parameter.

Geometry Optimization

In this work, one carbon atom is substituted by one aluminum atom (AlC_{31}) which corresponds to 3.125% of aluminum. Most theoretical investigations begin with optimizing the geometry of the species under examination.

A 4×4 pristine graphene consisting of 32 atoms were fully relaxed in xy plane, while z axis is kept 15Å. Both pure and doped graphene cell parameters were optimized. The cell parameter for optimized graphene sheet was 2.46Å which is similar to experimental [102, 103] and previous computational [104] works. The lattice parameters of 4×4 graphene supercell was increased to 9.84Å (four times the lattice parameter of graphene unit cell). In case of pristine graphene, the bond length C-C was found to be 1.4168Å after optimization which is almost close to the experimental value 1.421 Å [105]. The optimized lattice parameter vs total energy of undoped graphene is shown in figure 4.1a. The k points and energy cutoff are also optimized. Energy cutoff was converged at about 440 eV after optimization. Figure 4.2 shows the optimized structure for Al

doped graphene. Al is bonded to three C atoms by sp^2 hybridization. As shown in figure 4.2, the substitution C with Al had a considerable impact on the structure. After relaxation, C-C bond around Al is elongated while C-C bond far from Al was contracted. It is in the range of 1.40Å to 1.43Å. The bond length of Al-C is around 1.8547 Å which is almost similar to previous computational work [72, 106]. The Al-C bond length increase because of the large atomic radius of Al with respect to C. After geometry optimization and relaxation of the cell, self-consistent (SCF) calculation was performed by using $4 \times 4 \times 1$ k mesh. Then non-self-consistent (nSCF) calculation was done for band structure, DOS, and partial density of states (PDOS).
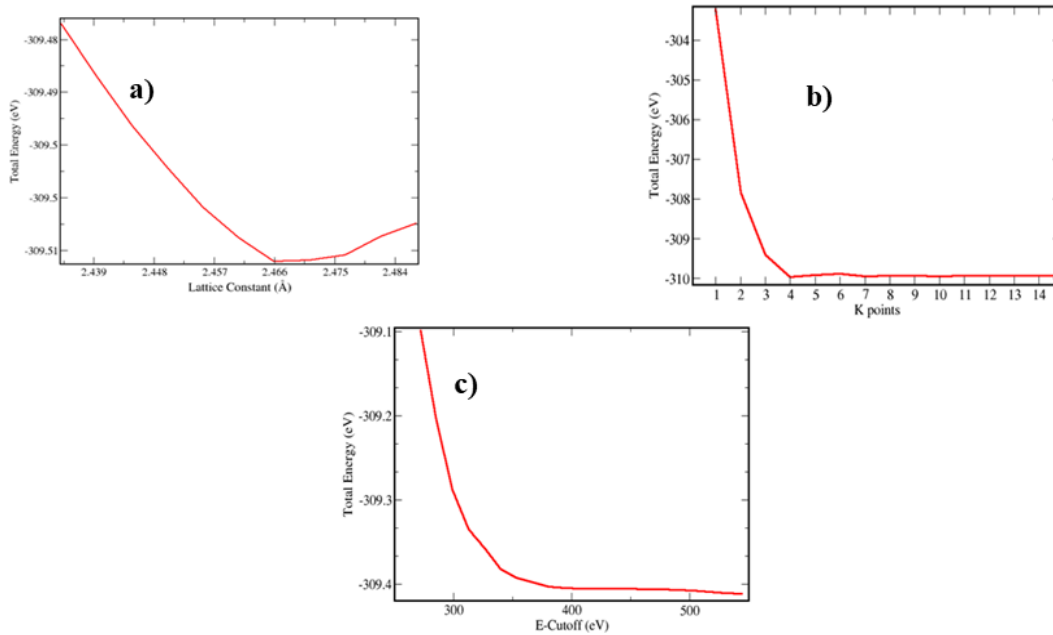

Figure 5. Geometry optimization of graphene a) lattice parameter optimization b) k-points optimization an c) energy cutoff optimization
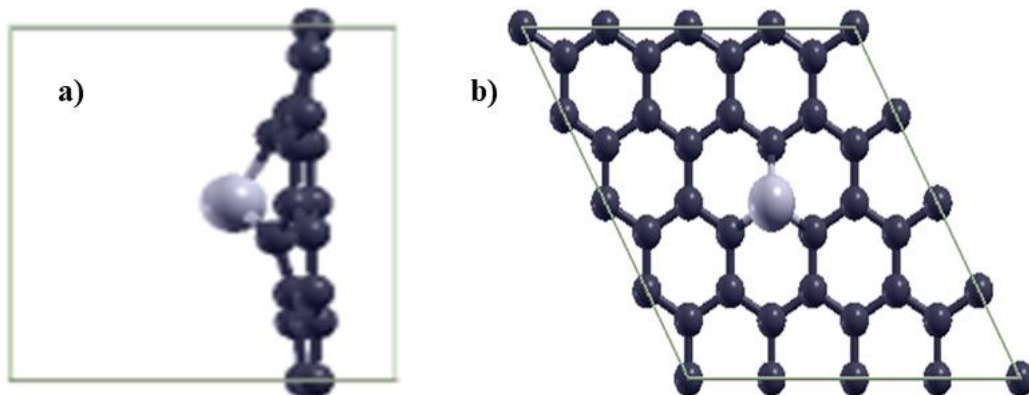
Figure 6. Optimized geometry of 4×4 Al doped graphene a) side view b) top view
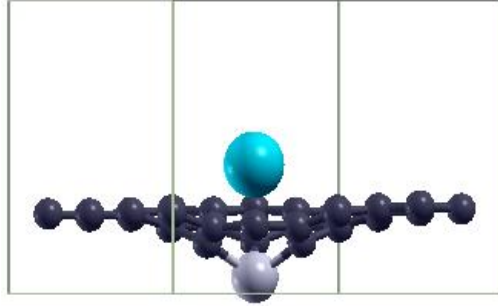
Figure 7. Optimized structure of single sodium ion on Al doped graphene (green Na, black C and brown Al atoms)

4.2 Formation Energy, Cohesive Energy and Adsorption Energy

4.2.1 Formation Energy

Formation energy is the potential energy due to the creation of vacancy or point defect. Formation energy of the Al doped graphene is calculated using equation 17. The calculated formation energy for Al doped graphene system is 11.51 eV.

4.2.2 Cohesive Energy

Cohesive energy is used to predict the stability of the structure. The cohesive energy of undoped graphene is given by the equation below.

$$E_{coh} = \frac{E_{gr-sheet} - n_c E_c}{n_C} \tag{20}$$

Where $E_{gr-sheet}$, E_c and n_C are total energy of graphene sheet, carbon atom and number of C atoms respectively. The calculated cohesive energy of pure graphene was $-8.5 eV/atom$.

For Al doped graphene

$$E_{coh} = \frac{E_{AlC} - (n_C E_C + n_{Al} E_{Al})}{n_C + n_{Al}} \tag{21}$$

Where E_{AlC}, E_{Al} and n_{Al} are total energy of Al doped graphene, energy of Al atoms and is number of Al atoms in the system. The calculated cohesive energy for Al doped graphene was $-7.84 eV/atom$. The negative sign of cohesive energy indicates that the system is stable.

4.2.3 Adsorption Energy

A vital for AlC_{31} monolayer for being a very appropriate negative electrode material for SIB is powerful adsorption of Na atom with the host substrate. It is an important property to understand the interaction between Na atoms and Al doped graphene. So, we have calculated adsorption energies of Na atom adsorbed on the AlC_{31} monolayer using equation 18.

The calculated adsorption energy $Na_x AlC_{31}$ where x concentration of Na atoms (it is integer from 1 to 9) was $-2.39 eV$, $-2.14 eV$, $-1.93 eV$, $-1.90 eV$, $-1.78 eV$, $-1.47 eV$, $-1.41 eV$, $-1.3 eV$, and $-1.2 eV$. The negative sign indicates that the absorbed Na on the AlC_{31} is stable. If number of Na atoms exceeds 9, adsorption become positive, and the structure is thermodynamically not stable.

The sign shows that the proposed material is a good anode for SIBs.

4.3 Storage Capacity and Open Circuit Voltage

Storage capacity (electrochemical performance) of electrode material is an important factor to determine whether the material is suitable electrode or not. To determine the storage capacity of Al doped graphene, the concentration of Na atoms are gradually increased until the adsorption energy become positive, because if adsorption energy is positive, the structure is no more stable. Equation 22 is used to calculate the storage capacity of Al doped graphene

$$C = \frac{nF}{3.6M} \tag{22}$$

where n, F and M are number of Na ion(s), Faraday constant ($96485.33 C/mol$) and Molar mass of Al doped graphene. 3.6 is used to convert coulombs mAh. The maximum sodium adsorbed is nine. By using equation 20, the theoretical capacity of our anode ($Na_9 AlC_{31}$) material is $604.05 mAh/g$

Open Circuit Voltage (OCV) is the other factor which determine the novelty of anode. It is used to study the storage property of the anode. Form adsorption energy we can simply calculate OCV by using the following equation.

$$OCV = -\frac{E_{ad}}{ze} \tag{23}$$

where z is the charge of Na ion (+1), and e is the charge of electron.

OCV of our anode material is decrease as concentration of Na ion increases. Based on the calculated adsorption energy, OCV of Na_xAlC_{31} was in the range of $0.75 - 1.494V$. This shows that the proposed material is a good anode for SIBs.

Average Voltage: Average Voltage is another important factor which is widely used to characterize the performance of our proposed material as an anode for SIBs. It can be calculated based on the equation below.

$$V = -\frac{E_{Na_xAlC_{31}} - E_{Na_{x-1}AlC_{31}} - (x - (x - 1))E_{Na}}{(x - (x - 1))e} \tag{24}$$

Based on this equation, the average voltage is when $x = 9$ (Na concentration is 9 and 8) is $0.64V$.

4.4 Electronic Properties

In this section, we try to investigate the effect of Al doping on the band structure and density of state of graphene monolayer. To calculate band structure 8×8×1 K points are used. And for DOS and PDOS, a dense 18×18×1 K point grid are used.

4.1.1 Band structure and Density of States

The electronic structure of graphene and aluminum doped graphene were computed by first-principle calculation.

The primary characteristics of electrical properties can be examined by looking at the two-dimensional (2D) band structures along high symmetry locations. At the K point, monolayer graphene possesses a Dirac-cone structure (Figure 8a). Figure 8b shows the band structure of graphene that is undoped. The band structure diagram of undoped graphene clearly reveals that the valence band (π) and conduction band (π*) of undoped graphene overlap at the Fermi energy level (E_F), resulting in a typical Dirac cone and graphene being a zero-band gap semiconductor

In terms of zero band gap and linear energy dispersion at the Fermi level, the computed band structure agrees well with the previously calculated band structure of graphene [107, 108]. As the state energy increases, the linear energy bands become parabolic dispersions.

When graphene is doped with Al atom (substitution), the fermi energy (E_F) level shifts to the valance band and linear dispersion of graphene disappeared (Figure 9). Al doping can be regarded as p-type doping, it modifies graphene into semiconductor.

The Partial density of states of doped graphene shows that the s orbital has less contribution in the valance band of doped graphene. P orbital has strong contribution for total density of states. But as energy increases, the contribution of s orbitals also increases. At around 7 eV the contribution of s
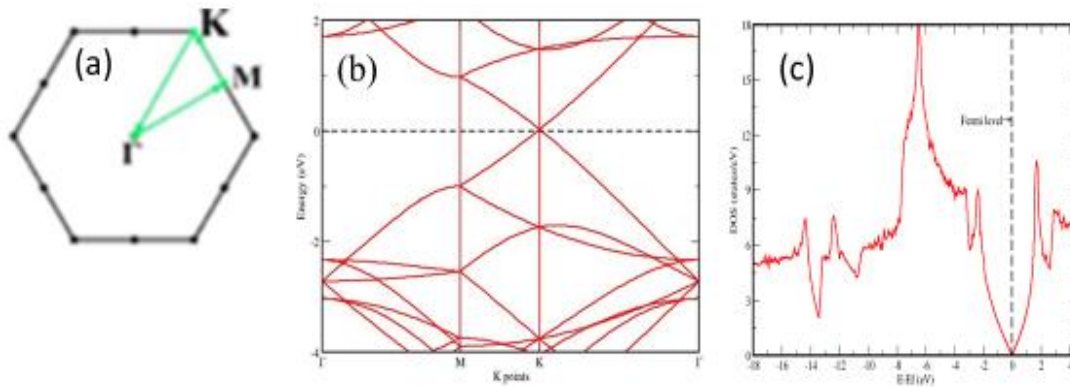

orbital is very high

Figure 8. 4×4×1 Graphene supercell a) FBZ and high symmetry point, b) band structure and c) DOS
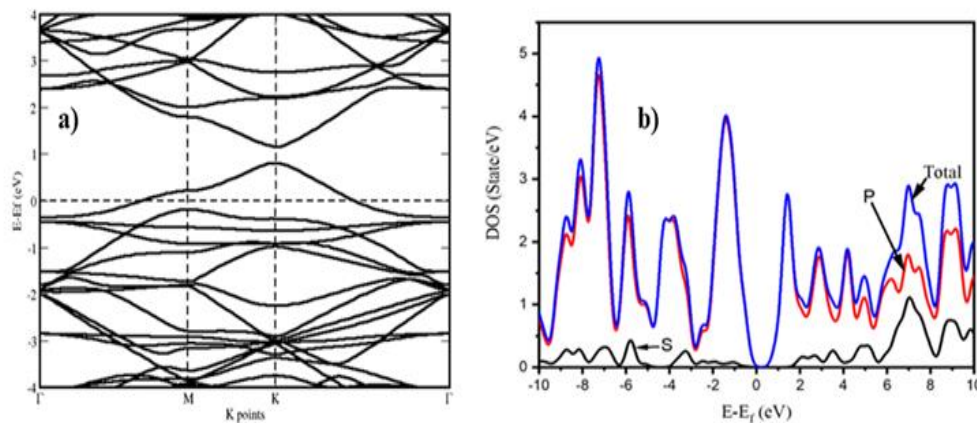
Figure 9. a) band structure and b) PDOS and total DOS of doped graphene supercell

4.4 Charge Distribution Analysis

To understand the interaction between Na ion and AlC_{31} monolayer during the charging and discharging process, nature of electronic transfer between Na ion and the surface of AlC_{31} was studied by using Bader charge algorithm

The doped Al into graphene modify the charge distribution around the carbon atoms. Table 1 shows the charge Al after doped on graphene. Since C is more electronegative than Al, it receives all the valance charge.

Table 1. Bader charge distribution analysis on Al doped graphene $Al - C$ distance between Al and C (d), Bader charge on Al atom $(Q_{Al}(e))$

$d\ (Al - C)$ (Å)	$Q_{Al}(e)$
1.8547	+2.1

The Bader charge analysis indicates that out of 127 valance electrons for aluminum doped graphene 0.896935 is assigned to Al and the rests are assigned to carbon. To convert this to ionic charge we have to check the number of core electrons (on-valance electrons). From Al and Carbon pseudopotential, we can get the valance configuration:

Table 2 .Valance Configuration of C

Nl	Pn	l	Occ	Rcut	Rcut US	E pseu
2S	1	0	2.00	1.00	1.200	-1.010678
2P	2	1	2.00	0.900	1.400	-0.388489

Table 3. Valance configuration of Al

Nl	Pn	l	Occ	Rcut	Rcut US	E pseu
3S	1	0	2.00	1.50	1.900	-0.569826
3P	2	1	2.00	1.500	1.900	-0.199337

The C pseudopotential indicates that two 1s electrons are fixed to the core. But Al pseudopotential indicates that two 1s, two 2s and six 2p electrons are fixed to the core.

The total number of electrons on Al is 2+2+6+0.896935 = 10.896935. By subtracting this these values from atomic numbers of Al (13) and C (4) we get Bader charge based ionic charge of state $Al^{2.1+}$ and $C^{0.9-.}$ This is smaller than the nominal ionic valance $+3$ for Al and -4 for Carbon which indicates that the system is covalent system.

For the system containing Na

Table 4. Properties of Single Na atom adsorbed on graphene surface: adsorption energy (E_a), Minimum distance between Na and Al doped graphene surface (h), Bader charge on Na ($QNa(e)$)

$E_a(eV\ Na\ on\ Al\ doped\ graphene)$	$h(Na-AlC)$ (Å)	$QNa(e)$
-2.39	2.54	$+0.9$

Table 5. Valance configuration of Na

Nl	Pn	L	Occ	Rcut	Rcut US	E pseu
2S	1	0	2.00	1.00	1.250	-4.158089
3S	2	0	1	1.00	1.250	-0.198813
2P	2	1	6.00	0.900	1.300	-2.106125

From Na pseudopotential, two 1s electron if fixed to the core. The total number of electrons on the Na is 2+8.100 = 10.1 thus, the charge on Na is 0.9e which shows the sodium is fully ionized. Na donates 0.9e to the substrate. The donated electron saturates the electron-deficient Aluminum carbon bond. It results in a chemical bonding between Al-doped graphene and Na+ ions. This indicates that there is a net charge transfer between the substrate and Na ions which indicates Al doped graphene can be used as anode

4.5 Diffusion of Na on the Surface of Al Doped Graphene

To be used in rechargeable batteries the anode material must exhibit a sufficiently low diffusion barrier in addition to suitable specific capacity, OCV, and adsorption energy values. The charge and discharge rate, which is crucial to the battery's performance, is controlled by the anode structures' electron transport and ion diffusion rates. Fast Na diffusion determines high charge

discharge rate of the battery. So, it is important to study the diffusion of Na on the surface of the doped graphene for its actual application.

In this study, NEB method is employed to study the diffusion barrier of Na on the surface of doped graphene. In order to find MEP, two equivalent positions are considered (Figure 10). Figure 10 shows the MEP and diffusion barrier of Na on the surface of doped graphene
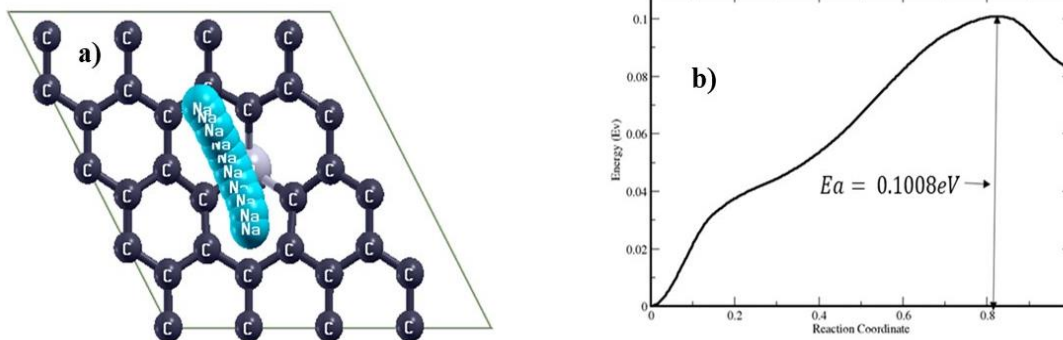
Figure 10. a) Possible pathway diffusion of Na and b) Diffusion energy barrier profile of Na over Al doped graphene

Figure 10(b) shows the diffusion barrier of Na on doped graphene. Here reaction coordinate indicates the distance between Na atom position at a given point along the diffusion pathways with respect to its starting position. Figure 11 shows that the barrier for Na diffusion along a given point is approximately 0.1eV. The calculated diffusion barrier is smaller than many proposed 2D anode for Na SIBs such as boron doped graphene (0.16-0.22 eV) [72], monolayer honeycomb borophene (0.17eV) [98], MoS_2 (0.28eV) [109] etc. The calculated diffusion energy barriers show promising results when compared to those of well-known heterostructure 2D materials, proving the value of Al doped graphene for use in SIBs. High charge and discharge rate is expected for this material to be used as an anode for SIBs.

5. CONCLUSION AND RECOMMENDATIONS

The computational method of materials simulation and modeling based on the DFT were used to study the property of doped and pristine graphene, adsorption and diffusion of Na ions on AlC_{31}. Maximum capacity, OCV and average voltage of AlC_{31} were investigated by using first principle calculation. AlC_{31} has negative adsorption energy for sodium ions. The $Na_x AlC_{31}$ has absorbing energies in the range of $-2.39eV$ to $-1.2eV$. The maximum specific capacity can reach $604.05mAh/g$ and larger than most of SIBs anode. It has OCV in the range of 0.75 to $1.494V$. The NEB calculation shows that AlC_{31} has low energy barrier (0.1008eV) for diffusion of for diffusion of Na ions. From all these calculations, it can be concluded that AlC_{31} is a excellent anode electrode material for SIBs.

Finally, we recommend that this electrode must be experimentally synthesized to be used in SIBs.

6. APPENDIX 1

6.1 NEB Calculation

Calculation of lowest energy path for a rearrangement of a group of atoms from one stable configuration to another is a common problem in theoretical chemistry and condensed matter physics [56, 57, 110]. Such a path is often referred to as the 'minimum energy path' (MEP) [56]. A common application of the MEP is to specify a "reaction coordinate" for transitions such as chemical reaction and diffusion process [56, 57]. The MEP may have one or more minima in between the endpoints corresponding to stable intermediate configurations. The MEP will then have two or more maxima, each one corresponding to a saddle point [57, 59]. The potential energy maximum along the MEP is the saddle point energy which gives the activation energy barrier [56]. Assuming a Boltzmann population is reached for the intermediate (meta) stable configurations, the overall rate is determined by the highest saddle point [57, 59, 110]. Computational methods for calculating MEPs are widely used in theoretical chemistry, physics, and materials science [58].

Many different methods have been presented for finding MEPs and saddle points [56, 57, 59, 110]. NEB method is an efficient technique to find MEP between two stable states of a transition [62].

The NEB is a chain of states method in which a string of images (geometric configurations of the
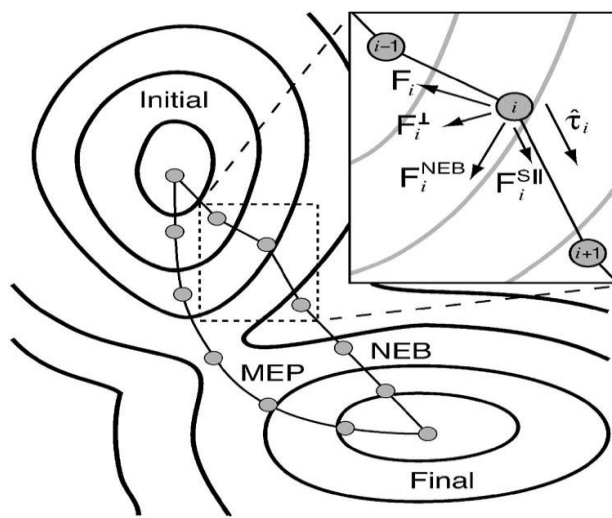
system) is used to describe a reaction pathway. These configurations are connected by spring forces to ensure equal spacing along the reaction path. Upon convergence of the NEB to the MEP, the images describe the reaction mechanism, up to the resolution of the images (Figure 11) [58].

Figure 11. Two components make up the nudged elastic band force

In NEB method, a string of replicas (or images) of the system are created and connected together with springs in such a way as to form a discrete representation of a path from the reactant configuration, R to product configuration, P. Initially, the images may be generated along the straight-line interpolation between R and P. An optimization algorithm is then applied to relax the images down towards the MEP. The string of images can be denoted by [R_0, R_1, R_2, . . ., R_N] where the endpoints are fixed and given by the initial and final states, R_0 = R and R_N = P, but N − 1 intermediate images are adjusted by the optimization algorithm. The simplest approach would be to create an object function and minimize with respect to intermediate images, R_1,…., R_N

$$S(R_1, \dots., R_n) = \sum_{i=1}^{N-1} E(R_i) + \sum_{i=1}^{N} \frac{k}{2}(R_i - R_{i-1})^2 \qquad (25)$$

This mimics an elastic band made up of $N - 1$ beads and N spring with spring constant k. The band is strung between the two fixed endpoints.

In the NEB method, the total force acting on an image is the sum of the spring force along the local tangent and the true force perpendicular to the local tangent

$$F_i^{NEB} = -\nabla E(R_i)|_\perp + F_i^S|_{||} \qquad (26)$$

where $\nabla E(R_i)$ is the gradient energy with respect to atomic coordinates in the system at image i and F_i^S is string force acting on image i. The perpendicular component of the gradient is obtained by subtracting out the parallel component

$$\nabla E(R_i)|_\perp = \nabla E(R_i) - \nabla E(R_i).\hat{\tau}_i \qquad (27)$$

where $\hat{\tau}_i$ is the normalized local tangent at image i.

In order to ensure equal spacing of the images (when the same spring constant, k, is used for all the springs), even in regions of high curvature where the angle between R_i − R_{i-1} and R_{i+1} − R_i deviates significantly from 0°, spring force is given by:

$$F_i^S|_{||} = k(|R_{i+1} - R_i| - |R_i - R_{i-1}|)\hat{\tau}_i \tag{28}$$

An optimization algorithm is then used to move the images according to the force in equation 26. In equation 28, R_i is the position of ith image.

7. REFERENCES

[1]   S. Qi, D. Wu, Y. Dong, J. Liao, C. W. Foster, C. O'Dwyer, Y. Feng, C. Liu, and J. Ma, "Cobalt-based electrode materials for sodium-ion batteries," Chemical Engineering Journal, vol. 370, pp. 185-207, 2019.

[2]   L. Wang, Y. Wang, M. Wu, Z. Wei, C. Cui, M. Mao, J. Zhang, X. Han, Q. Liu, and J. Ma, "Nitrogen, fluorine, and boron ternary doped carbon fibers as cathode electrocatalysts for zinc–air batteries," Small, vol. 14, no. 20, pp. 1800737, 2018.

[3]   Y. Ma, Q. Guo, M. Yang, Y. Wang, T. Chen, Q. Chen, X. Zhu, Q. Xia, S. Li, and H. Xia, "Highly doped graphene with multi-dopants for high-capacity and ultrastable sodium-ion batteries," Energy Storage Materials, vol. 13, pp. 134-141, 2018.

[4]   Y. Fang, Z. Chen, L. Xiao, X. Ai, Y. Cao, and H. Yang, "Recent progress in iron-based electrode materials for grid-scale sodium-ion batteries," Small, vol. 14, no. 9, pp. 1703116, 2018.

[5]   K. Chayambuka, G. Mulder, D. L. Danilov, and P. H. Notten, "Sodium-ion battery materials and electrochemical properties reviewed," Advanced Energy Materials, vol. 8, no. 16, pp. 1800079, 2018.

[6]   C. Chen, Y. Wen, X. Hu, X. Ji, M. Yan, L. Mai, P. Hu, B. Shan, and Y. Huang, "Na+ intercalation pseudocapacitance in graphene-coupled titanium oxide enabling ultra-fast sodium storage and long-term cycling," Nature communications, vol. 6, no. 1, pp. 1-8, 2015.

[7]   H. Dua, J. Deb, D. Paul, and U. Sarkar, "Twin-graphene as a Promising Anode Material for Na-Ion Rechargeable Batteries," ACS Applied Nano Materials, vol. 4, no. 5, pp. 4912-4918, 2021.

[8]   T. Hwang, M. Cho, and K. Cho, "Interlayer Design of Pillared Graphite by Na-Halide Cluster Intercalation for Anode Materials of Sodium-Ion Batteries," ACS omega, vol. 6, no. 14, pp. 9492-9499, 2021.

[9]   H. Jia, C. Chen, O. Oladele, Y. Tang, G. Li, X. Zhang, and F. Yan, "Cobalt doping of tin disulfide/reduced graphene oxide nanocomposites for enhanced pseudocapacitive sodium-ion storage," Communications Chemistry, vol. 1, no. 1, pp. 1-12, 2018.

[10]   S. Yang, S. Li, S. Tang, W. Dong, W. Sun, D. Shen, and M. Wang, "Sodium adsorption and intercalation in bilayer graphene from density functional theory calculations," Theoretical Chemistry Accounts, vol. 135, no. 7, pp. 1-11, 2016.

[11]   G. Yang, P. R. Ilango, S. Wang, M. S. Nasir, L. Li, D. Ji, Y. Hu, S. Ramakrishna, W. Yan, and S. Peng, "Carbon-Based Alloy-Type Composite Anode Materials toward Sodium-Ion Batteries," Small, vol. 15, no. 22, pp. 1900628, 2019.

[12]   T. D. Pham, H. D. Luong, K. Sato, Y. Shibutani, and V. A. Dinh, "Two-dimensional Na x SiS as a promising anode material for rechargeable sodium-based batteries: ab initio material design," Physical Chemistry Chemical Physics, vol. 21, no. 44, pp. 24326-24332, 2019.

[13]   T. Perveen, M. Siddiq, N. Shahzad, R. Ihsan, A. Ahmad, and M. I. Shahzad, "Prospects in anode materials for sodium ion batteries-A review," Renewable and Sustainable Energy Reviews, vol. 119, pp. 109549, 2020.

[14]   I. Hasa, X. Dou, D. Buchholz, Y. Shao-Horn, J. Hassoun, S. Passerini, and B. Scrosati, "A sodium-ion battery exploiting layered oxide cathode, graphite anode and glyme-based electrolyte," Journal of Power Sources, vol. 310, pp. 26-31, 2016.

[15]   S. Yang, S. Li, S. Tang, D. Shen, W. Dong, and W. Sun, "Adsorption, intercalation and diffusion of Na on defective bilayer graphene: a computational study," Surface Science, vol. 658, pp. 31-37, 2017.

[16]   S. A. Aslanzadeh, "A computational study on the potential application of zigzag carbon nanotubes in Mg-ion batteries," Structural Chemistry, vol. 31, no. 3, pp. 1073-1078, 2020.

[17]   Y. Yang, D.-M. Tang, C. Zhang, Y. Zhang, Q. Liang, S. Chen, Q. Weng, M. Zhou, Y. Xue, and J. Liu, ""Protrusions" or "holes" in graphene: which is the better choice for sodium ion storage?," Energy & Environmental Science, vol. 10, no. 4, pp. 979-986, 2017.

[18]   S.-M. Zheng, Y.-R. Tian, Y.-X. Liu, S. Wang, C.-Q. Hu, B. Wang, and K.-M. Wang, "Alloy anodes for sodium-ion batteries," Rare Metals, vol. 40, no. 2, pp. 272-289, 2021.

[19]   S. Yasar, İ. Söğütlü, H. Mert, N. Mert, E. Vessally, and Y. Lin, "Zigzag and armchair AlN nanotubes as anode materials for Mg-ion batteries: Computational study," Solid State Sciences, vol. 110, pp. 106448, 2020.

[20]   N. Ortiz-Vitoriano, N. E. Drewett, E. Gonzalo, and T. Rojo, "High performance manganese-based layered oxide cathodes: overcoming the challenges of sodium ion batteries," Energy & Environmental Science, vol. 10, no. 5, pp. 1051-1074, 2017.

[21]   K. C. Wasalathilake, H. Li, L. Xu, and C. Yan, "Recent advances in graphene based materials as anode materials in sodium-ion batteries," Journal of Energy Chemistry, vol. 42, pp. 91-107, 2020.

[22]   Z. Deng, Y. Mo, and S. P. Ong, "Computational studies of solid-state alkali conduction in rechargeable alkali-ion batteries," NPG Asia Materials, vol. 8, no. 3, pp. e254-e254, 2016.

[23]   H. An, Y. Li, Y. Gao, C. Cao, J. Han, Y. Feng, and W. Feng, "Free-standing fluorine and nitrogen co-doped graphene paper as a high-performance electrode for flexible sodium-ion batteries," Carbon, vol. 116, pp. 338-346, 2017.

[24]   K. Belasfar, A. El Kenz, and A. Benyoussef, "First-principles study of BC7 monolayer an ultra-high capacity anode for lithium-ion and sodium-ion batteries applications," Materials Chemistry and Physics, vol. 257, pp. 123751, 2021.

[25]   Y. Li, M. Chen, B. Liu, Y. Zhang, X. Liang, and X. Xia, "Heteroatom doping: an effective way to boost sodium ion storage," Advanced Energy Materials, vol. 10, no. 27, pp. 2000927, 2020.

[26]   J. Ye, H. Zhao, W. Song, N. Wang, M. Kang, and Z. Li, "Enhanced electronic conductivity and sodium-ion adsorption in N/S co-doped ordered mesoporous carbon for high-performance sodium-ion battery anode," Journal of Power Sources, vol. 412, pp. 606-614, 2019.

[27]   Q. Bai, L. Yang, H. Chen, and Y. Mo, "Computational studies of electrode materials in sodium-ion batteries," Advanced energy materials, vol. 8, no. 17, pp. 1702998, 2018.

[28]   Q. He, B. Yu, Z. Li, and Y. Zhao, "Density functional theory for battery materials," Energy & Environmental Materials, vol. 2, no. 4, pp. 264-279, 2019.

[29]   Y. Ma, "Computer simulation of cathode materials for lithium ion and lithium batteries: A review," Energy & Environmental Materials, vol. 1, no. 3, pp. 148-173, 2018.

[30]   R. Dan, W. Chen, Z. Xiao, P. Li, M. Liu, Z. Chen, and F. Yu, "N-Doped biomass carbon/reduced graphene oxide as a high-performance anode for sodium-ion batteries," Energy & Fuels, vol. 34, no. 3, pp. 3923-3930, 2020.

[31]   L. Fan, X. Li, X. Song, N. Hu, D. Xiong, A. Koo, and X. Sun, "Promising dual-doped graphene aerogel/SnS2 nanocrystal building high performance sodium ion batteries," ACS applied materials & interfaces, vol. 10, no. 3, pp. 2637-2648, 2018.

[32]   S. Gong, and Q. Wang, "Boron-doped graphene as a promising anode material for potassium-ion batteries with a large capacity, high rate performance, and good cycling stability," The Journal of Physical Chemistry C, vol. 121, no. 44, pp. 24418-24424, 2017.

[33]   N. Argaman, and G. Makov, "Density functional theory: An introduction," American Journal of Physics, vol. 68, no. 1, pp. 69-79, 2000.

[34]   P. J. Hasnip, K. Refson, M. I. Probert, J. R. Yates, S. J. Clark, and C. J. Pickard, "Density functional theory in the solid state," Philosophical Transactions of the Royal Society A: Mathematical, Physical and Engineering Sciences, vol. 372, no. 2011, pp. 20130270, 2014.

[35]   D. Bagayoko, "Understanding density functional theory (DFT) and completing it in practice," AIP Advances, vol. 4, no. 12, pp. 127104, 2014.

[36]   G. Samsonidze, and B. Kozinsky, "Accelerated screening of thermoelectric materials by first-principles computations of electron–phonon scattering," Advanced Energy Materials, vol. 8, no. 20, pp. 1800246, 2018.

[37]   L. Brancaleon, "Chapter Four - Combined Use of Optical Spectroscopy and Computational Methods to Study the Binding and the Photoinduced Conformational Modification of Proteins When NMR and X-Ray Structural Determinations Are Not an Option," Advances in Protein Chemistry and Structural Biology, C. Z. Christov, ed., pp. 95-152: Academic Press, 2013.

[38]   C. Bradley, and A. Cracknell, The mathematical theory of symmetry in solids: representation theory for point groups and space groups: Oxford University Press, 2010.

[39]   M. O'Keeffe, and B. G. Hyde, Crystal structures: Courier Dover Publications, 2020.

[40]   R.-J. Slager, A. Mesaros, V. Juričić, and J. Zaanen, "The space group classification of topological band-insulators," Nature Physics, vol. 9, no. 2, pp. 98-102, 2013.

[41]   B. t. Champagne, E. A. Perpète, S. J. Van Gisbergen, E.-J. Baerends, J. G. Snijders, C. Soubra-Ghaoui, K. A. Robins, and B. Kirtman, "Assessment of conventional density functional schemes for computing the polarizabilities and hyperpolarizabilities of conjugated oligomers: An ab initio investigation of polyacetylene chains," The Journal of chemical physics, vol. 109, no. 23, pp. 10489-10498, 1998.

[42] R. J. Abraham, L. Griffiths, and P. Loftus, "Approaches to charge calculations in molecular mechanics," Journal of Computational Chemistry, vol. 3, no. 3, pp. 407-416, 1982.

[43] P. J. Winn, G. G. Ferenczy, and C. A. Reynolds, "Toward improved force fields. 1. Multipole-derived atomic charges," The Journal of Physical Chemistry A, vol. 101, no. 30, pp. 5437-5445, 1997.

[44] D. L. Mobley, C. I. Bayly, M. D. Cooper, M. R. Shirts, and K. A. Dill, "Small molecule hydration free energies in explicit solvent: an extensive test of fixed-charge atomistic simulations," Journal of chemical theory and computation, vol. 5, no. 2, pp. 350-358, 2009.

[45] J. D. Thompson, J. D. Xidos, T. M. Sonbuchner, C. J. Cramer, and D. G. Truhlar, "More reliable partial atomic charges when using diffuse basis sets," PhysChemComm, vol. 5, no. 18, pp. 117-134, 2002.

[46] A. E. Reed, R. B. Weinstock, and F. Weinhold, "Natural population analysis," The Journal of chemical physics, vol. 83, no. 2, pp. 735-746, 1985.

[47] G. Henkelman, A. Arnaldsson, and H. Jónsson, "A fast and robust algorithm for Bader decomposition of charge density," Computational Materials Science, vol. 36, no. 3, pp. 354-360, 2006.

[48] E. Sanville, S. D. Kenny, R. Smith, and G. Henkelman, "Improved grid-based algorithm for Bader charge allocation," Journal of computational chemistry, vol. 28, no. 5, pp. 899-908, 2007.

[49] F. L. Hirshfeld, "Bonded-atom fragments for describing molecular charge densities," Theoretica chimica acta, vol. 44, no. 2, pp. 129-138, 1977.

[50] T. A. Manz, and N. G. Limas, "Introducing DDEC6 atomic population analysis: part 1. Charge partitioning theory and methodology," RSC advances, vol. 6, no. 53, pp. 47771-47801, 2016.

[51] A. V. Marenich, S. V. Jerome, C. J. Cramer, and D. G. Truhlar, "Charge model 5: An extension of Hirshfeld population analysis for the accurate description of molecular interactions in gaseous and condensed phases," Journal of chemical theory and computation, vol. 8, no. 2, pp. 527-541, 2012.

[52] B. H. Besler, K. M. Merz Jr, and P. A. Kollman, "Atomic charges derived from semiempirical methods," Journal of computational chemistry, vol. 11, no. 4, pp. 431-439, 1990.

[53] W. Tang, E. Sanville, and G. Henkelman, "A grid-based Bader analysis algorithm without lattice bias," Journal of Physics: Condensed Matter, vol. 21, no. 8, pp. 084204, 2009.

[54] I. Choudhuri, and D. G. Truhlar, "Calculating and characterizing the charge distributions in solids," Journal of Chemical Theory and Computation, vol. 16, no. 9, pp. 5884-5892, 2020.

[55] H. Jónsson, G. Mills, and K. W. Jacobsen, "Nudged elastic band method for finding minimum energy paths of transitions," 1998.

[56] B. J. Berne, G. Ciccotti, and D. F. Coker, Classical and quantum dynamics in condensed phase simulations: Proceedings of the International School of Physics: World Scientific, 1998.

[57] G. Henkelman, G. Jóhannesson, and H. Jónsson, "Methods for finding saddle points and minimum energy paths," Theoretical methods in condensed phase chemistry, pp. 269-302: Springer, 2002.

[58] D. Sheppard, R. Terrell, and G. Henkelman, "Optimization methods for finding minimum energy paths," The Journal of chemical physics, vol. 128, no. 13, pp. 134106, 2008.

[59] G. Henkelman, B. P. Uberuaga, and H. Jónsson, "A climbing image nudged elastic band method for finding saddle points and minimum energy paths," The Journal of chemical physics, vol. 113, no. 22, pp. 9901-9904, 2000.

[60] D. Alhat, V. Lasrado, and Y. Wang, "A review of recent phase transition simulation methods: Saddle point search." pp. 103-111.

[61] E. d. V. Gómez, S. Amaya-Roncancio, L. B. Avalle, D. H. Linares, and M. C. Gimenez, "DFT study of adsorption and diffusion of atomic hydrogen on metal surfaces," Applied Surface Science, vol. 420, pp. 1-8, 2017.

[62] D. Giri, H. E. Kadiri, and C. Barrett, "Twin nucleation in Ti: A study using nudged elastic band (NEB) method," arXiv preprint arXiv:2201.12444, 2022.

[63] H. Tian, Z. W. Seh, K. Yan, Z. Fu, P. Tang, Y. Lu, R. Zhang, D. Legut, Y. Cui, and Q. Zhang, "Theoretical investigation of 2D layered materials as protective films for lithium and sodium metal anodes," Advanced Energy Materials, vol. 7, no. 13, pp. 1602528, 2017.

38

[64] Y.-X. Li, D. B. Putungan, and S.-H. Lin, "Two-dimensional MTe2 (M= Co, Fe, Mn, Sc, Ti) transition metal tellurides as sodium ion battery anode materials: Density functional theory calculations," Physics Letters A, vol. 382, no. 38, pp. 2781-2786, 2018.

[65] M. I. Khan, G. Nadeem, A. Majid, and M. Shakil, "A DFT study of bismuthene as anode material for alkali-metal (Li/Na/K)-ion batteries," Materials Science and Engineering: B, vol. 266, pp. 115061, 2021.

[66] S. Ullah, P. A. Denis, and F. Sato, "Adsorption and diffusion of alkali-atoms (Li, Na, and K) on BeN dual doped graphene," International Journal of Quantum Chemistry, vol. 119, no. 11, pp. e25900, 2019.

[67] K. C. Wasalathilake, G. A. Ayoko, and C. Yan, "Effects of heteroatom doping on the performance of graphene in sodium-ion batteries: A density functional theory investigation," Carbon, vol. 140, pp. 276-285, 2018.

[68] L. Chen, Y. Hernandez, X. Feng, and K. Müllen, "From nanographene and graphene nanoribbons to graphene sheets: chemical synthesis," Angewandte Chemie International Edition, vol. 51, no. 31, pp. 7640-7654, 2012.

[69] E. Olsson, G. Chai, M. Dove, and Q. Cai, "Adsorption and migration of alkali metals (Li, Na, and K) on pristine and defective graphene surfaces," Nanoscale, vol. 11, no. 12, pp. 5274-5284, 2019.

[70] J. Hassoun, F. Bonaccorso, M. Agostini, M. Angelucci, M. G. Betti, R. Cingolani, M. Gemmi, C. Mariani, S. Panero, and V. Pellegrini, "An advanced lithium-ion battery based on a graphene anode and a lithium iron phosphate cathode," Nano letters, vol. 14, no. 8, pp. 4901-4906, 2014.

[71] H. Xu, H. Chen, and C. Gao, "Advanced graphene materials for sodium/potassium/aluminum-ion batteries," ACS Materials Letters, vol. 3, no. 8, pp. 1221-1237, 2021.

[72] C. Ling, and F. Mizuno, "Boron-doped graphene as a promising anode for Na-ion batteries," Physical Chemistry Chemical Physics, vol. 16, no. 22, pp. 10419-10424, 2014.

[73] B. Mortazavi, A. Dianat, O. Rahaman, G. Cuniberti, and T. Rabczuk, "Borophene as an anode material for Ca, Mg, Na or Li ion storage: a first-principle study," Journal of Power Sources, vol. 329, pp. 456-461, 2016.

[74]   B. C. Saha, A. K. Bera, and S. M. Yusuf, "Mechanism of Na-Ion Conduction in the Highly Efficient Layered Battery Material Na2Mn3O7," ACS Applied Energy Materials, vol. 4, no. 6, pp. 6040-6054, 2021.

[75]   J.-Y. Hwang, S.-T. Myung, and Y.-K. Sun, "Sodium-ion batteries: present and future," Chemical Society Reviews, vol. 46, no. 12, pp. 3529-3614, 2017.

[76]   H. Zhang, Y. Huang, H. Ming, G. Cao, W. Zhang, J. Ming, and R. Chen, "Recent advances in nanostructured carbon for sodium-ion batteries," Journal of Materials Chemistry A, vol. 8, no. 4, pp. 1604-1630, 2020.

[77]   W. Zhang, F. Zhang, F. Ming, and H. N. Alshareef, "Sodium-ion battery anodes: Status and future trends," EnergyChem, vol. 1, no. 2, pp. 100012, 2019.

[78]   H. Lee, K. Paeng, and I. S. Kim, "A review of doping modulation in graphene," Synthetic Metals, vol. 244, pp. 36-47, 2018.

[79]   D. Ma, and Z. Yang, "First-principles studies of Pb doping in graphene: stability, energy gap and spin–orbit splitting," New Journal of Physics, vol. 13, no. 12, pp. 123018, 2011.

[80]   L.-H. Yao, M.-S. Cao, H.-J. Yang, X.-J. Liu, X.-Y. Fang, and J. Yuan, "Adsorption of Na on intrinsic, B-doped, N-doped and vacancy graphenes: A first-principles study," Computational materials science, vol. 85, pp. 179-185, 2014.

[81]   D. S. Sholl, and J. A. Steckel, Density functional theory: a practical introduction: John Wiley & Sons, 2011.

[82]   A. S. Rad, "Al-doped graphene as modified nanostructure sensor for some ether molecules: Ab-initio study," Synthetic Metals, vol. 209, pp. 419-425, 2015.

[83]   A. S. Rad, "Al-doped graphene as a new nanostructure adsorbent for some halomethane compounds: DFT calculations," Surface Science, vol. 645, pp. 6-12, 2016.

[84]   Y. Tian, J. Ren, W. Yue, M. Chen, G. Hu, and X. Yuan, "Adsorption of chloroform on N-doped and Al-doped graphene: A first-principle study," Chemical Physics Letters, vol. 685, pp. 344-348, 2017.

[85]   M. D. Esrafili, N. Saeidi, and P. Nematollahi, "A DFT study on SO3 capture and activation over Si-or Al-doped graphene," Chemical Physics Letters, vol. 658, pp. 146-151, 2016.

[86]   A. S. Rad, and V. P. Foukolaei, "Density functional study of Al-doped graphene nanostructure towards adsorption of CO, CO2 and H2O," Synthetic Metals, vol. 210, pp. 171-178, 2015.

[87] F. Montejo-Alvaro, J. Oliva, M. Herrera-Trejo, H. Hdz-García, and A. Mtz-Enriquez, "DFT study of small gas molecules adsorbed on undoped and N-, Si-, B-, and Al-doped graphene quantum dots," Theoretical Chemistry Accounts, vol. 138, no. 3, pp. 1-15, 2019.

[88] Z. Zheng, and H. Wang, "Different elements doped graphene sensor for CO2 greenhouse gases detection: The DFT study," Chemical Physics Letters, vol. 721, pp. 33-37, 2019.

[89] Z. Ao, S. Li, and Q. Jiang, "Thermal stability of interaction between the CO molecules and the Al doped graphene," Physical Chemistry Chemical Physics, vol. 11, no. 11, pp. 1683-1687, 2009.

[90] X. Qin, Q. Meng, and W. Zhao, "Effects of Stone–Wales defect upon adsorption of formaldehyde on graphene sheet with or without Al dopant: a first principle study," Surface Science, vol. 605, no. 9-10, pp. 930-933, 2011.

[91] X.-Y. Liu, J.-M. Zhang, K.-W. Xu, and V. Ji, "Improving SO2 gas sensing properties of graphene by introducing dopant and defect: a first-principles study," Applied surface science, vol. 313, pp. 405-410, 2014.

[92] S. F. Rastegar, A. A. Peyghan, and N. L. Hadipour, "Response of Si-and Al-doped graphenes toward HCN: a computational study," Applied surface science, vol. 265, pp. 412-417, 2013.

[93] T. Chen, L. An, and X. Jia, "A DFT-based analysis of adsorption properties of fluoride anion on intrinsic, B-doped, and Al-doped graphene," Journal of Molecular Modeling, vol. 27, no. 2, pp. 1-11, 2021.

[94] D. Cortés-Arriagada, and A. Toro-Labbé, "Aluminum and iron doped graphene for adsorption of methylated arsenic pollutants," Applied Surface Science, vol. 386, pp. 84-95, 2016.

[95] J. Gu, X. Zhang, L. Fu, and A. Pang, "Study on the hydrogen storage properties of the dual active metals Ni and Al doped graphene composites," International Journal of Hydrogen Energy, vol. 44, no. 12, pp. 6036-6044, 2019.

[96] A. K. Sahoo, and M. R. Panigrahi, "A study on strain and density in graphene-induced Bi2O3 thin film," Bulletin of Materials Science, vol. 44, no. 3, pp. 1-9, 2021.

[97] P. Rani, G. S. Dubey, and V. Jindal, "DFT study of optical properties of pure and doped graphene," Physica E: Low-dimensional Systems and Nanostructures, vol. 62, pp. 28-35, 2014.

[98] J. Li, G. A. Tritsaris, X. Zhang, B. Shi, C. Yang, S. Liu, J. Yang, L. Xu, J. Yang, and F. Pan, "Monolayer honeycomb borophene: A promising anode material with a record capacity for lithium-ion and sodium-ion batteries," Journal of The Electrochemical Society, vol. 167, no. 9, pp. 090527, 2020.

[99] P. Bhauriyal, A. Mahata, and B. Pathak, "Graphene-like carbon–nitride monolayer: a potential anode material for Na-and K-ion batteries," The Journal of Physical Chemistry C, vol. 122, no. 5, pp. 2481-2489, 2018.

[100] J. Su, Y. Pei, Z. Yang, and X. Wang, "Ab initio study of graphene-like monolayer molybdenum disulfide as a promising anode material for rechargeable sodium ion batteries," RSC Advances, vol. 4, no. 81, pp. 43183-43188, 2014.

[101] A. G. Garcia, S. E. Baltazar, A. H. R. Castro, J. F. P. Robles, and A. Rubio, "Influence of S and P doping in a graphene sheet," Journal of Computational and Theoretical Nanoscience, vol. 5, no. 11, pp. 2221-2229, 2008.

[102] M. Z. Flores, P. A. Autreto, S. B. Legoas, and D. S. Galvao, "Graphene to graphane: a theoretical study," Nanotechnology, vol. 20, no. 46, pp. 465704, 2009.

[103] B. D. Kong, S. Paul, M. B. Nardelli, and K. W. Kim, "First-principles analysis of lattice thermal conductivity in monolayer and bilayer graphene," Physical Review B, vol. 80, no. 3, pp. 033406, 2009.

[104] S. Ullah, A. Hussain, W. Syed, M. A. Saqlain, I. Ahmad, O. Leenaerts, and A. Karim, "Band-gap tuning of graphene by Be doping and Be, B co-doping: a DFT study," RSC advances, vol. 5, no. 69, pp. 55762-55773, 2015.

[105] H. Yanagisawa, T. Tanaka, Y. Ishida, M. Matsue, E. Rokuta, S. Otani, and C. Oshima, "Phonon dispersion curves of a B C 3 honeycomb epitaxial sheet," Physical review letters, vol. 93, no. 17, pp. 177003, 2004.

[106] A. S. Rad, "First principles study of Al-doped graphene as nanostructure adsorbent for NO2 and N2O: DFT calculations," Applied Surface Science, vol. 357, pp. 1217-1224, 2015.

[107] N. T. T. Tran, D. K. Nguyen, O. E. Glukhova, and M.-F. Lin, "Coverage-dependent essential properties of halogenated graphene: A DFT study," Scientific reports, vol. 7, no. 1, pp. 1-13, 2017.

[108] M. Asadov, S. Guseinova, and V. Lukichev, "Ab Initio Modeling of the Electronic and Energy Structure and Opening the Band Gap of a 4p-Element-Doped Graphene Monolayer," Russian Microelectronics, vol. 49, no. 5, pp. 314-323, 2020.

[109] M. Mortazavi, C. Wang, J. Deng, V. B. Shenoy, and N. V. Medhekar, "Ab initio characterization of layered MoS2 as anode for sodium-ion batteries," Journal of Power Sources, vol. 268, pp. 279-286, 2014.

[110] S. D. Schwartz, Theoretical methods in condensed phase chemistry: Springer Science & Business Media, 2002.